ARTICLE IN PRESS

Computers and Mathematics with Applications ▮ (▮▮▮▮) ▮▮▮–▮▮▮

Contents lists available at ScienceDirect

Computers and Mathematics with Applications

journal homepage: www.elsevier.com/locate/camwa

Instability of smoothed particle hydrodynamics applied to Poiseuille flows

Baofang Song [a,1], Arman Pazouki [b], Thorsten Pöschel [a,*]

[a] Institute for Multiscale Simulation, Friedrich-Alexander-Universität Erlangen-Nürnberg, Nägelsbachstraße 49b, 91052 Erlangen, Germany

[b] Department of Mechanical Engineering, California State University at Los Angeles, Los Angeles, CA, USA

ARTICLE INFO

Article history:
Received 7 September 2017
Received in revised form 25 March 2018
Accepted 25 June 2018
Available online xxxx

Keywords:
Smoothed particle hydrodynamics
Simple shear
Instability

ABSTRACT

Smoothed particle hydrodynamics (SPH) has been widely applied to flows with free surface, multi-phase flow, and systems with complex boundary geometry. However, it has been shown that SPH suffers from transverse instability when applied to simple wall-bounded shear flows such as Poiseuille and Couette flows at moderate and high Reynolds number, $\mathrm{Re} \gtrsim 1$, casting the application of SPH to practical situations into doubt, where the Reynolds number is frequently large. Here, we consider Poiseuille flows for a wide range of Reynolds number and find that the documented instability of SPH can be avoided by using appropriate ratio of smoothing length to particle spacing in combination with a density re-initialization technique, which has not been systematically investigated in simulations of simple shear flows. We also probe the source of the instability and point out the limitations of SPH for wall-bounded shear flows at high Reynolds number.

1. Introduction

Originally, *smoothed particle hydrodynamics* (SPH) was proposed to solve astrophysical problems [1,2]; however, by now there is a much wider range of applications. Because of its meshless and particle-based nature, it is frequently applied to fluid flows with free surfaces [3–6], multi-phase systems [4,3,7,8], and systems with complex boundary geometry [9]. Very recently it was also applied to particle laden flow by fully resolving the flow around moving solid particles [10,11] and wall-bounded turbulence [12]. For a comprehensive review on the fundamentals and applications of SPH see [13–15]. Within the SPH paradigm, there are two different approaches to handle incompressible flow problems, namely *incompressible SPH* (ISPH) which imposes incompressibility by solving the pressure Poisson equation [4,16–20] and *weekly compressible SPH* (WCSPH), which exploits an equation of state to relate density and pressure and approximately imposes the incompressibility by assigning high speed of sound. Mainly because of its pure Lagrangian nature and computational simplicity, WCSPH was extensively used for various flow simulations, e.g. [3,4,9,21,10,11,5,6,12]. In this paper, we refer to WCSPH as SPH and focus on its application to incompressible wall-bounded shear flow.

For shear flow at low Reynolds numbers, SPH yields satisfactory results [9,10,21–23]. However, for larger Reynolds numbers, SPH fails, in particular in simulations of simple shear flow [24,22,25,23]. Imaeda & Inutsuka [24] argued that in standard SPH the particle velocity cannot exactly represent the fluid velocity, therefore, density error gradually increases and invalidates the simulation results. Similar to a recent transport-velocity formulation for SPH [8], the solution provided

* Corresponding author.
E-mail address: thorsten.poeschel@fau.de (T. Pöschel).

[1] Present address: Center for Applied Mathematics, Tianjin University, Tianjin 300072, China.

https://doi.org/10.1016/j.camwa.2018.06.037
0898-1221/

in [24] relies on two velocities, i.e. the particle and fluid velocities. However, the Lagrangian property of SPH is lost in those formulations.

For plane Poiseuille flow, Basa et al. [25] investigated the performance of various viscous force formulations, boundary condition implementations, and particle inconsistency corrections in SPH and observed that the failure of the method cannot be avoided even at a very low Reynolds number, Re $\approx$ 1. The authors identified the inherent inability of SPH to suppress transverse fluctuations as the source of the failure, in agreement with earlier studies [22,26], and termed the instability as *transverse instability*. The same source of failure was found by Meister et al. [23] who considered plane Poiseuille and Couette flows. Although they showed a convergence for small Reynolds number, the numerical error was still considerable ($\approx$ 10% for Re=65). These findings also suggested that the specific choice of kernel function is irrelevant to the failure of the method, as the same type of instability occurs with different kernel functions (B-spline kernel in [25] and quintic spline kernel in [23]). Besides, it is also concluded by these authors that regular initial particle distributions are intrinsically unstable with respect to transverse fluctuations in Poiseuille and Couette flows [23].

The appearance of the instability poses fundamental limitation of the application of SPH to wall-bounded shear flows. We identify the sensitivity of the particle discretization accuracy on particle distribution as the source of the instability and propose strategies to achieve a satisfactory performance of classical SPH simulations. In this paper we also systematically study the effects of method parameters, background pressure, initial particle configurations, and a density re-initialization technique on the performance of SPH for simple shear flow and pipe flow at Reynolds numbers between Re $\approx$ 0.01 and 100.

2. SPH methods

SPH is a Lagrangian approach to solve the Navier–Stokes equations numerically using discrete quasi-particles. The discretization scheme is further elaborated in the following sub-sections.

2.1. Continuity equation

The evolution of density can be formulated using the continuity equation

$$\frac{d\rho}{dt} = -\rho\nabla\cdot\vec{v}, \tag{1}$$

where ρ and $\vec{v}$ are the fluid density and velocity, respectively. In the formulation of SPH, Eq. (1) reads

$$\frac{d\rho_a}{dt} = \rho_a \sum_b \frac{m_b}{\rho_b}\left(\vec{v}_a - \vec{v}_b\right)\cdot\nabla_a W_{ab}\,, \tag{2}$$

where ρ_a is the density of particle a, m_b is the mass of particle b and ∇_a denotes the derivative with respect to the position $\vec{r}_a$ of particle a. W is the kernel function, and $W_{ab} \equiv W\left(\vec{r}_a - \vec{r}_b, h\right)$. In this paper, the cubic spline kernel function given in [10] with a compact support is employed, which reads

$$W\left(\vec{r}, h\right) = \frac{1}{4\pi h^3}\begin{cases}(2-q)^3 - 4(1-q)^3, & 0 \le q < 1,\\ (2-q)^3, & 1 \le q < 2,\\ 0, & q \ge 2,\end{cases} \tag{3}$$

where $q \equiv \left|\vec{r}\,\right|/h$. Alternatively, the density can also be directly obtained using

$$\rho_a = \sum_b m_b W_{ab}\,. \tag{4}$$

Both types of density updating schemes, Eqs. (2) and (4), yield similar results [25]; however, usually the former is preferred as it produces smoother density fields in the vicinity of boundaries [10,21]. In this paper, we adopt the continuity equation Eq. (2) together with a density re-initialization technique using Eq. (4) [4,10].

2.2. Momentum equation

The momentum equation reads

$$\frac{d\vec{v}}{dt} = -\frac{1}{\rho}\nabla p + \frac{\mu}{\rho}\nabla^2\vec{v} + \vec{f}, \tag{5}$$

where p is the pressure and $\vec{f}$ denotes the external body force density. Regarding discretization, we apply the gradient and viscous term formulation given in [7,9]:

$$\left(-\frac{1}{\rho}\nabla p\right)_a = -\frac{1}{m_a}\sum_b (V_a^2 + V_b^2)\tilde{p}_{ab}\nabla_a W_{ab} \tag{6}$$

$$\left(\frac{\mu}{\rho}\nabla^2\vec{v}\right)_a = \frac{1}{m_a}\sum_b \left(V_a^2 + V_b^2\right)\tilde{\mu}_{ab}\frac{\vec{r}_{ab}\cdot\nabla_a W_{ab}}{|\vec{r}_{ab}|^2 + \epsilon h^2}\left(\vec{v}_a - \vec{v}_b\right) \tag{7}$$

Please cite this article in press as: B. Song, et al., Instability of smoothed particle hydrodynamics applied to Poiseuille flows, Computers and Mathematics with Applications (2018), https://doi.org/10.1016/j.camwa.2018.06.037.

where $V_a \equiv m_a/\rho_a$ is the volume of particle a, and

$$\tilde{p}_{ab} \equiv \frac{\rho_a p_b + \rho_b p_a}{\rho_a + \rho_b}; \qquad \tilde{\mu}_{ab} \equiv 2\frac{\mu_a \mu_b}{\mu_a + \mu_b} \tag{8}$$

are the inter-particle-averaged pressure and viscosity associated with particles a and b. The term ϵh^2 in the denominator of Eq. (7), where h is the length scale of the smoothing kernel and ϵ is a small number (usually $\epsilon = 0.01$), is introduced to avoid the singularity when $\left|\vec{r}_{ab}\right| \to 0$.

In our simulations we tested also alternative formulations for the pressure gradient and the viscous term proposed in [10,21] and no significant difference was observed.

2.3. Equation of state

The equation of state [13],

$$p = p_0 \left[\left(\frac{\rho}{\rho_0} \right)^{\gamma} - 1 \right], \tag{9}$$

relates pressure and density. Here, p is the dynamic pressure and $p_0 \equiv c^2\rho_0/\gamma$, with the numerical speed of sound, c, which should be large compared to the flow speed in order to keep the density variation small. We chose c 10 times the maximum velocity of the steady Poiseuille flow. Typically $\gamma = 7$ [13], although other values, e.g., $\gamma = 1$ have also been used [8,27]. In our tests, simulation results are insensitive of the numerical value of γ. In the following, we only show the results with $\gamma = 7$.

2.4. No-slip boundary condition

The no-slip boundary condition is achieved by using dummy particles located outside of the flow domain. We chose the implementation proposed in [9] which has been shown robust. The properties of dummy particles are not updated according to Navier–Stokes equations. They are rather updated based on the following procedure: first, the fluid velocity is extrapolated to the position of wall dummy particles to obtain $\hat{\vec{v}}$,

$$\hat{\vec{v}} = \frac{\sum \vec{v}_{\text{fluid}} W}{\sum W} \tag{10}$$

then the velocity of the wall dummy particles is calculated via

$$\vec{v} = 2\vec{v}_{\text{wall}} - \hat{\vec{v}}\,. \tag{11}$$

The pressure of the dummy particles is approximated from the ambient fluid as $p_{\text{wall}} = \sum p_{\text{fluid}} W \big/ \sum W$, and finally the density of dummy particles is calculated according to the equation of state, Eq. (9). For the update of density using Eq. (2), the actual wall velocity, $\vec{v}_{\text{wall}}$, is assigned to the dummy particles instead of using Eq. (11), see [9].

The problem with the boundary condition is that the position of the wall surface in simulation where $\vec{v} = 0$ may not coincide with the physical wall surface everywhere as it will be determined by the velocity extrapolation and may vary in time, depending on the particle distribution near the wall. While this problem is inherent to general wall modeling of SPH, there exist implementations that can accurately reconstruct the no-slip velocity condition at simple boundaries like flat plates or spherical boundary (e.g., [28]). Nevertheless, this effect can be systematically reduced by increasing the spatial resolution. Further numerical errors appear due to the boundary pressure approximation.

3. Failure of SPH applied to plane Poiseuille flow

Using the method described in Section 2, we simulate plane Poiseuille flow in three dimensions with periodic boundary condition in the flow direction and spanwise direction. Initially the flow is at rest and driven by a constant external force. The system is integrated in time using a 2nd-order Runge–Kutta scheme [10] and the criteria of [8,23] are used to control the time-step size, which is

$$\Delta t = \frac{1}{4} \min \left\{ \frac{h}{c + |\mathrm{v}_{\max}|}, \frac{h^2}{\nu}, \sqrt{\frac{h}{|f|}} \right\}, \tag{12}$$

where f is the external force, ν is the kinematic viscosity of the fluid and $\mathrm{v}_{\max}$ is the characteristic velocity. The Reynolds number is defined as $\mathrm{Re} = H\mathrm{v}_{\max}/2\nu$ where H is the channel gap width and herein $\mathrm{v}_{\max}$ is the maximum velocity of the steady Poiseuille flow under a given driving force. Herein, we chose the reference density $\rho_0 = 1000\,\mathrm{kg/m^3}$, $\nu = 10^{-4}\,\mathrm{m^2/s}$ and $H = 0.2\,\mathrm{m}$. We use small computational domains with spanwise width 0.025 m and streamwise length 0.06 m and impose periodic boundary condition in these two directions. We vary the body force density, f, to vary the terminal velocity and, thus, the terminal Reynolds number assumed for $t \to \infty$. The numerical results are compared with the analytical

Please cite this article in press as: B. Song, et al., Instability of smoothed particle hydrodynamics applied to Poiseuille flows, Computers and Mathematics with Applications (2018), https://doi.org/10.1016/j.camwa.2018.06.037.

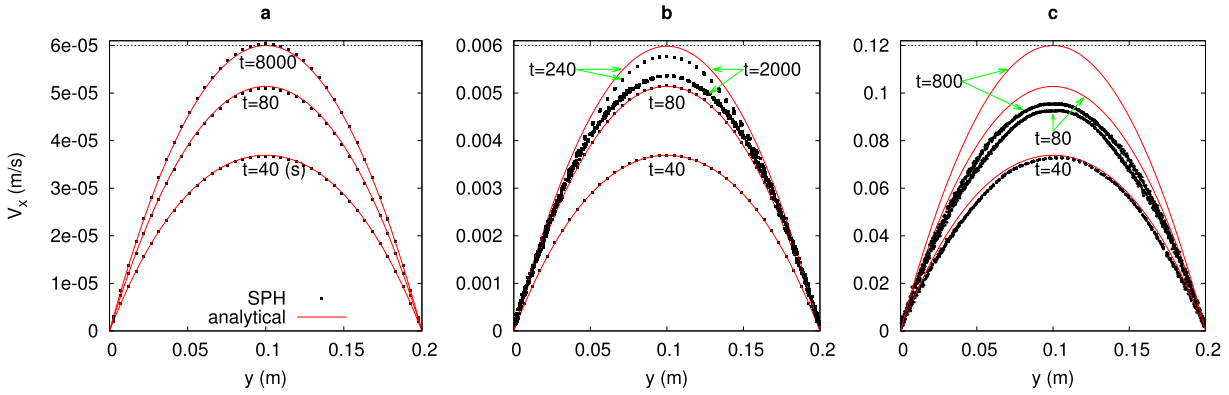

Fig. 1. Failure of SPH in transient plane Poiseuille flow. Velocity profiles of plane Poiseuille flow for (a) Re = 0.06, (b) Re = 6, and (c) Re = 120 at different time, t, starting at rest at $t = 0$. The symbols show the streamwise velocity of all SPH particles versus their position in the direction normal to the wall. The lines show the analytical solution [22].

solution of the transient Poiseuille flow under constant body force [21]. Using the described geometry and viscosity, the analytical solution will assume its steady state, i.e., the parabolic laminar flow profile, at time $t \gtrsim 240$ s.

We consider three values of the Reynolds number, Re $= \{0.06, 6, 120\}$, the peak velocity at the channel center is $v_{max} = 6 \times 10^{-5}$ m/s, 6×10^{-3} m/s and 1.2×10^{-1} m/s, respectively, and the corresponding driving pressure gradient $f = 1.2 \times 10^{-6}$ m/s^2, 1.2×10^{-4} m/s^2 and 2.4×10^{-3} m/s^2, respectively. The driving pressure gradient f is applied suddenly to the fluid at rest. The characteristic length scale associated with the kernel function h, referred to as the smoothing length, is normally a measure of spatial resolution, and is used to determine the particle spacing Δx. We first consider the typical case of $h/\Delta x = 1$. Fig. 1a shows the velocity profiles due to the numerical and analytical solutions.

At Re $= 0.06$, for all times, the simulation results agree with the transient analytical solutions [22] up to a good accuracy. The largest time, $t = 8000$ s (corresponding to $2.4H/v_{max}$), is plotted against the stationary solution. The error may be quantified by means of the L_2 norm

$$L_2 = \sqrt{\frac{\sum_{\{N\}} \left[v_x - U_x\left(\vec{r}\right)\right]^2 + v_y^2 + v_z^2}{\sum_{\{N\}} \left[U_x\left(\vec{r}\right)\right]^2}}, \tag{13}$$

where $\vec{v} = \left(v_x, v_y, v_z\right)$ are the velocity components in the streamwise, wall normal and spanwise directions, and $U_x\left(\vec{r}\right)$ is the analytical streamwise velocity at the (particle) position $\vec{r}$. The summation is performed over all N fluid particles at positions $\vec{r}$ traveling at velocity of $\vec{v}$. The stationary solution for Re $= 0.06$ shown in Fig. 1a corresponds to $L_2 = 0.8\%$.

For intermediate Reynolds number, Re $= 6$, we use the parameters $h/H = 0.025$ and $h/\Delta x = 1$. Fig. 1b shows the corresponding profiles of the velocity obtained from the simulation in comparison with the analytical result. Again, at $t = 0$ the flow starts at rest. For short time, when velocity is far below the asymptotic value, analytical and numerical velocity profiles agree well. For larger time, $t = 240$ s, when the analytical solution converged to the stationary state; however, large deviations between the analytical and numerical solutions appear. For yet larger time, the SPH solution deviates further from the analytical steady state solution and seems to converge to a blunted velocity profile at about $t = 2000$ s. Besides, we also observed a characteristic evolution of the fluctuations of the velocity profile: the velocity field first becomes noisy near the walls; later the noise spreads out from the near wall region to almost the entire flow domain, see Fig. 1b. This is different from the case Re $= 0.06$ where the particles stay aligned in rows during the entire simulation, see Fig. 1a.

Poiseuille flow at high Reynolds numbers is rarely discussed in the literature. Here we perform simulations for Re $= 120$. The parameters are $h/H = 0.02$ and $h/\Delta x = 1$. It has been shown that SPH simulations fail at relatively large Reynolds number [23,25] which is in agreement with our simulation shown in Fig. 1c. Here we observe large deviations between analytical and numerical simulations even for $t = 40$ s, including large noise, asymmetry of the velocity profile and a non-physical plateau at the channel center.

We find that increasing the spatial resolution (decreasing the smoothing length h) does not solve the problem. Fig. 2 shows the L_2-error, according to Eq. (13), for Re $= 6$ and Re $= 120$ using smoothing length $h/H = \{0.01, 0.015, 0.02, 0.025\}$. For both *Re*'s, we observed rapid increase of the error regardless of the resolution. For Re $= 6$, the L_2 even does not converge. Clearly, reducing the smoothing length does not noticeably improve the stability, which is in agreement with [25]. We believe that the smoothing length has only minor influence on the stability, if any. The results suggest that SPH fails at Reynolds number Re $\gtrsim 1$, in agreement with [22,23,25].

We wish to point out that the described effects: noisy flow field, blunted velocity profile, and large L_2 in the stationary state, are not the effects of turbulence since the Reynolds number is far lower than the lowest Reynolds number at which turbulence can be observed in plane Poiseuille flow (about 700 [29]).

Please cite this article in press as: B. Song, et al., Instability of smoothed particle hydrodynamics applied to Poiseuille flows, Computers and Mathematics with Applications (2018), https://doi.org/10.1016/j.camwa.2018.06.037.

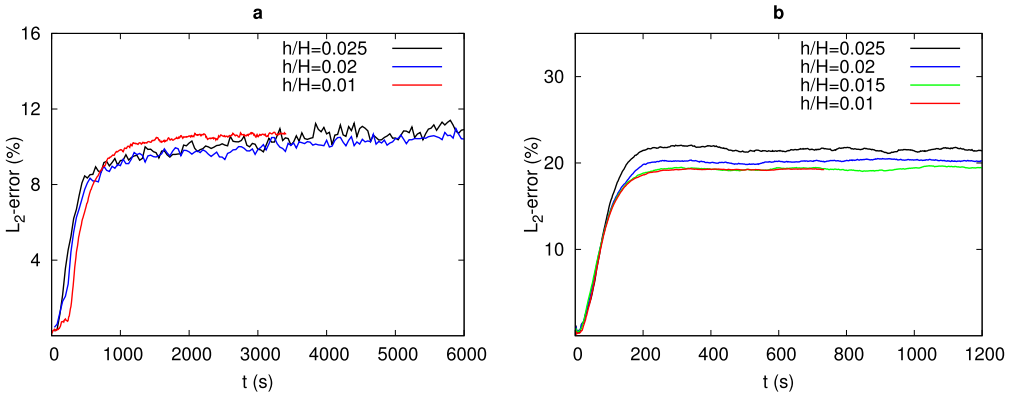

Fig. 2. Evolution of the L_2 error given by Eq. (13) for different smoothing lengths, h. (a) Poiseuille flow at Re = 6; (b) at Re = 120.

4. Strategies to avoid the instability

The failure of SPH in plane Poiseuille flow, reported previously [22,23,25] and also shown in Section 3 restricts the applicability of the method to systems with very small Reynolds number. In this section, we test measures to improve the stability of SPH.

We believe that the wall boundary condition implementation (see Section 2.4) introduces perturbations of the velocity field near the wall, which is unavoidable in general SPH modeling [15], and causes particles to undergo transverse drift. Under shear, the (cross-shear) transverse drift of particles will cause inhomogeneity of the particle distribution [25] and undermine the particle discretization accuracy of SPH [30] (this effect is not observed at Re = 0.06 because it takes very long time for the inhomogeneity to develop at very low speeds, and also may not be significant in non-shear-dominating flow problems). We conjecture that the deterioration of the particle discretization accuracy causes the instability for larger flow velocity. Therefore, in order to improve the stability of SPH, it is essential to keep a good particle discretization accuracy for a given spatial resolution.

4.1. Influence of the background pressure

It is central to keep the homogeneity of the particle distribution for a good particle discretization accuracy, which however is a difficult task in SPH. Background pressure can to some extent regularize the particle distribution and is often used to avoid clustering of particles in SPH simulations, the so-called tensile instability [31]. Here we test a few values of background pressure, 0.025 p_0, 0.05 p_0, and 0.1 p_0, where $p_0 = c^2\rho_0/\gamma$, see Eq. (9), for Poiseuille flow with parameters Re=120, $h/H = 0.02$, and $h/\Delta x = 1$.

As known, SPH is not gauge-invariant with respect to background pressure, i.e., the results will be different given different background pressure [9]. Indeed, we observed sensitive dependence on the background pressure, see Fig. 3. 0.05 p_0 gives good convergence at later time, while the error increases significantly with other two values. Even for 0.05 p_0 the error increases rapidly during the transient development of the Poiseuille flow. It is also clear that an improper choice of background pressure can lead to an unphysical velocity profile, see the 0.1 p_0 case in Fig. 3b which manifests an unphysical velocity plateau near the channel center (similar plateau is also present for smaller p_0, although weaker). More importantly, there is no a priori rule for a proper choice of background pressure, which likely is problem dependent.

4.2. Influence of smoothing length to particle spacing ratio, $h/\Delta x$

This parameter determines the neighbor list size of a particle. For a cubic spline, the smoothing kernel function [10] used in this paper, $h/\Delta x = 1$ corresponds to about 30 neighbor particles. In case of regular and homogeneous particle distribution, we find that the typical value $h/\Delta x = 1$ gives good accuracy (see the case of Re = 0.06). However, when inhomogeneity occurs in particle distribution, the particle discretization accuracy is undermined. Intuitively, this can be improved by including more neighbor particles into consideration, i.e., increasing $h/\Delta x$. Fig. 4 shows L_2 over time for $h/\Delta x = \{1, 1.3, 1.5\}$, again for Re = 6 and Re = 120. We choose the smoothing length $h/H = 0.025$ for Re = 6 and $h/H = 0.02$ for Re = 120. We observe drastic reduction of the L_2-error with increasing $h/\Delta x$ for both cases, Re = 6 and Re = 120. While for $h/\Delta x = 1$ and $h/\Delta x = 1.3$ the error is still unacceptably large and keeps increasing, for $h/\Delta x = 1.5$ we obtain $L_2 < 2\%$ in the entire time domain for Re = 6 and $L_2 < 5\%$ for Re = 120. The significant influence of $h/\Delta x$ for Poiseuille flow is in line with earlier results by Ellero and Adams [32], who computed the friction forces acting on a cylinder confined in channel flow using SPH and found $h/\Delta x \gtrsim 1.5$ necessary for converged results.

Please cite this article in press as: B. Song, et al., Instability of smoothed particle hydrodynamics applied to Poiseuille flows, Computers and Mathematics with Applications (2018), https://doi.org/10.1016/j.camwa.2018.06.037.

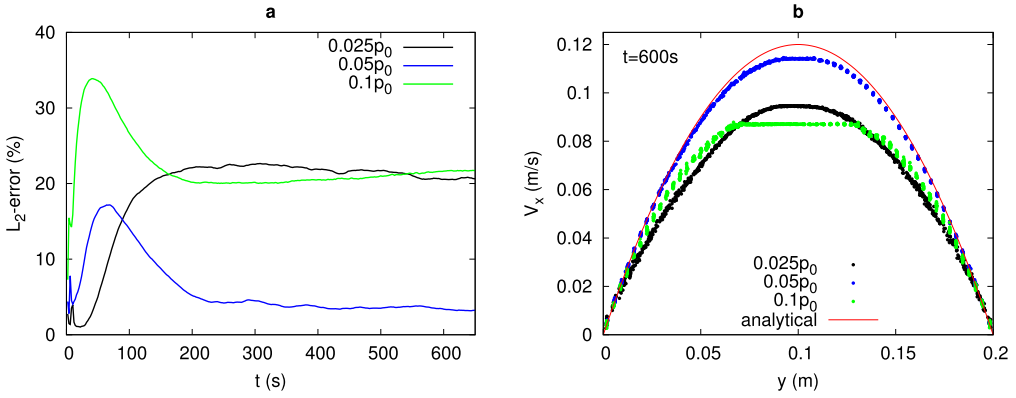

Fig. 3. (Color online) Simulation results for Poiseuille flow (Re $= 120$, $h/H = 0.02$, $h/\Delta x = 1$) at different background pressure values, $0.025\,p_0$ (black), $0.05\,p_0$ (blue), and $0.1\,p_0$ (green). (a) Evolution of the L_2 error; (b) velocity profiles at $t = 600$ s. The symbols show the streamwise velocity of all SPH particles versus their position in the direction normal to the wall. Lines show analytical solutions.

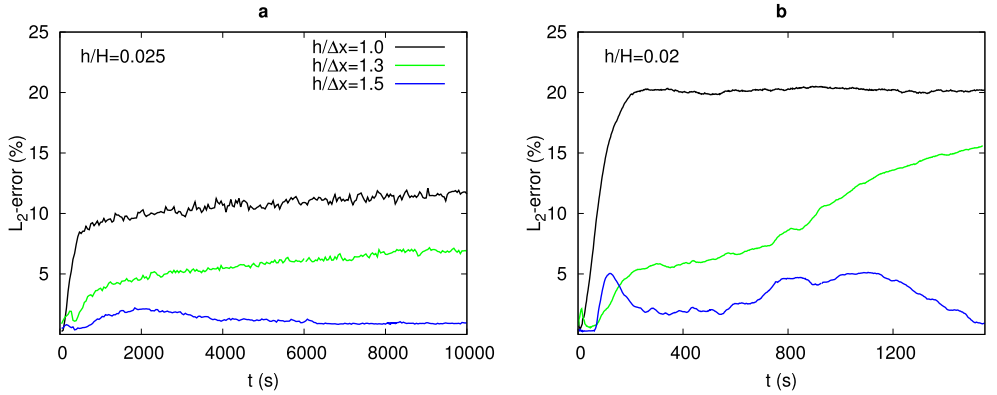

Fig. 4. Evolution of the L_2 error given by Eq. (13) for different ratios of smoothing lengths to particle spacing, $h/\Delta x$. (a) Poiseuille flow at Re $= 6$; (b) at Re $= 120$.

4.3. Influence of the initial particle distribution

In many SPH simulations, the initial particle positions are chosen regularly, e.g. located on a rectangular or triangular lattice. It is suggested, however, that this choice of initial conditions may contribute to instability of the numerical solution [23,25]. In order to investigate the influence of the initial conditions, we compare the numerical results obtained using initial positions where the particles start at rest from a rectangular lattice with the results using irregular initial conditions. The irregular particle setup is generated in the following way: particles start from lattice positions but at random velocity, then the system is relaxed by solving the Navier–Stokes equations in the absence of the external body force until the maximum velocity in the domain is below 10^{-9} m/s, when we consider the relaxation of the particle position has finished. There are other ways of generating non-lattice particle configurations, such as the packing method by [33]. Fig. 5 shows L_2 over time for regular and irregular initial conditions for Re $= 120$.

As expected, both simulations lead to identical stationary states, that is, the same L_2 value up to fluctuations. The accuracy of the transient flow is, however, slightly better for the case of regular initial positions, thus, we cannot confirm the argument presented in [23,25] that lattice configuration of SPH particles contributes to the instability. In fact, the instability could occur to both configurations. However, irregular particle configuration produced in similar ways may generate better results in other systems, such as in Taylor–Green vortices [8]. This issue seems to be problem dependent.

4.4. Influence of density re-initialization

Updating density via the continuity equation, Eq. (2), can result in an inconsistency of mass, density and the volume occupied by the particles [4,21], given fixed particle mass. Morris et al. [21] pointed out that this is not important for flow at low Reynolds number (see also our results at Re $= 0.06$), however, at larger Reynolds number, this inconsistency may lead to a noisy flow field and inaccurate results [4]. Considerable improvement could be achieved using the density re-initialization

Please cite this article in press as: B. Song, et al., Instability of smoothed particle hydrodynamics applied to Poiseuille flows, Computers and Mathematics with Applications (2018), https://doi.org/10.1016/j.camwa.2018.06.037.

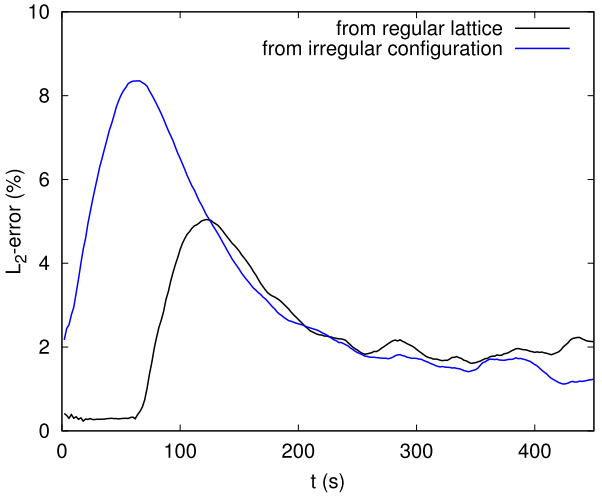

Fig. 5. Evolution of the L_2 error given by Eq. (13) for Poiseuille flow at Re $= 120$ ($h/H = 0.02$ and $h/\Delta x = 1.5$) with different initial particle settings.

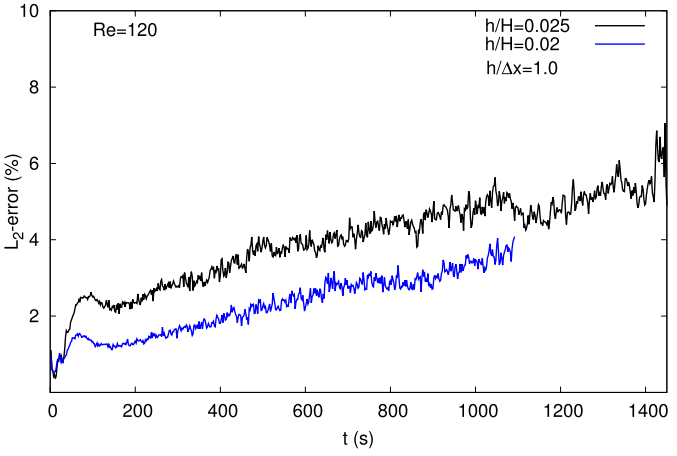

Fig. 6. Evolution of the L_2 error for Poiseuille flow (Re $= 120$, $h/H = 0.025$ and 0.02 with $h/\Delta x = 1.0$) using the density re-initialization technique.

technique [4]. This technique aims to improve the density field obtained from Eq. (2) by frequently using the direct density summation in Eq. (4). Similar techniques are also used to improve stability in other types of moving particle simulations (MPS) [34,35]. This technique involves a summation over all particles and increases the computation costs. Fortunately this correction only needs to be performed at a much lower frequency than the time-stepping. Usually this technique is performed every 10 or 20 time steps [4,10,23]. Colagrossi et al. [4] tested the effects of the re-initialization frequency and showed that a frequency around 20 shows a good performance in terms of total kinetic energy conservation.

Fig. 6 shows the effect of the density re-initialization for Re=120 with $h/H = 0.025$ and 0.02 and $h/\Delta x = 1.0$, it is clear that the density re-initialization significantly suppresses the error compared to the case without this technique as shown by the black line in Fig. 2b; however, the L_2 error keeps growing as the simulation carries on. This implies that density re-initialization alone cannot well suppress the instability for long time simulations.

Fig. 7a shows the deviation of the simulation result from the analytical solution L_2 for Re $= 120$ ($h/H = 0.02$, $h/\Delta x = 1.5$) when applying the density re-initialization technique together with the zeroth order correction of the density summation [10,23], which is important near solid boundaries where the support of fluid particles is incomplete.

We find that density re-initialization, combined with $h/\Delta x = 1.5$, reduces L_2 by almost an order of magnitude to $L_2 < 1\%$ for the entire simulation. Moreover, the stationary velocity profile obtained from SPH agrees well with the analytical solution, see Fig. 7b. For further evaluation, Fig. 8a shows the fluctuations of density, revealing a reduction of almost an order of magnitude when applying density re-initialization. Similarly, the fluctuations of pressure are reduced as well, as shown in Fig. 8b, evidently due to the relation between pressure and density through the equation of state in SPH. Finally, Fig. 8c,d

Please cite this article in press as: B. Song, et al., Instability of smoothed particle hydrodynamics applied to Poiseuille flows, Computers and Mathematics with Applications (2018), https://doi.org/10.1016/j.camwa.2018.06.037.

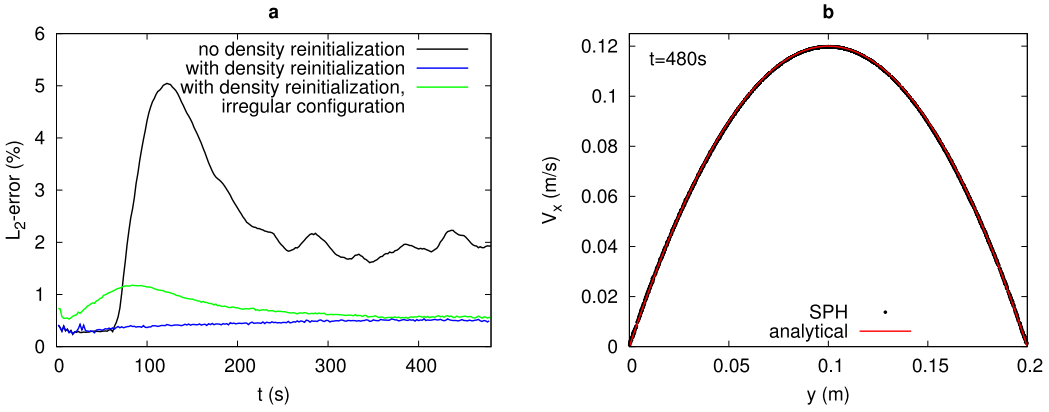

Fig. 7. Simulation results for Poiseuille flow (Re $= 120$, $h/H = 0.02$, $h/\Delta x = 1.5$). (a) Evolution of the L_2 error with and without density re-initialization. (b) Velocity profiles at $t = 480\,s$ obtained from SPH with density re-initialization in comparison with the analytical solution. The symbols show the streamwise velocity of all SPH particles versus their position in the direction normal to the wall.

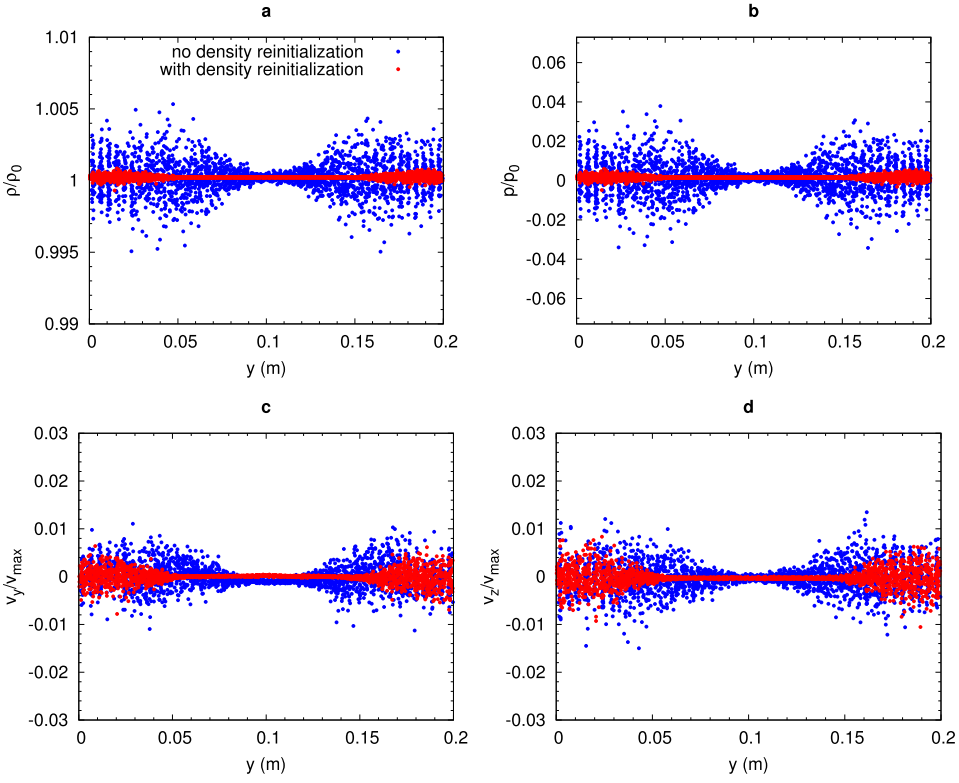

Fig. 8. Influence of density re-initialization on the obtained hydrodynamic fields for Poiseuille flow at Re $= 120$ ($h/H = 0.02$, $h/\Delta x = 1.5$). The figures compare the simulation results with and without density re-initialization. (a) density normalized by the reference density, $\rho_0 = 1000\,kg/m^3$; (b) pressure normalized by $p_0 = c^2\rho_0/\gamma$; (c) velocity normal to the wall normalized by v_{max}; (d) spanwise velocity normalized by v_{max}. Data are taken at $t = 120\,s$ when the difference of the L_2 values are maximal, see Fig. 7a.

show the transverse velocity fluctuations in the flow domain, which illustrates the regularization of the velocity field due to applying the density re-initialization technique. Choosing the numerical speed of sound to be 10 times the maximum flow velocity (0.12 m/s), the density variation obtained from the simulation without density re-initialization is below 1%. However, the transverse velocity fluctuations close to the wall boundary can reach above 1% of the centerline velocity. Density re-initialization reduces the velocity fluctuations. Nevertheless, this effect is only significant far from the wall where the fluctuations almost vanish, see Fig. 8c,d. Velocity fluctuations near the wall boundary are not significantly reduced which is due to the fact that they are rooted in the inaccurate boundary velocity and pressure approximation.

Please cite this article in press as: B. Song, et al., Instability of smoothed particle hydrodynamics applied to Poiseuille flows, Computers and Mathematics with Applications (2018), https://doi.org/10.1016/j.camwa.2018.06.037.

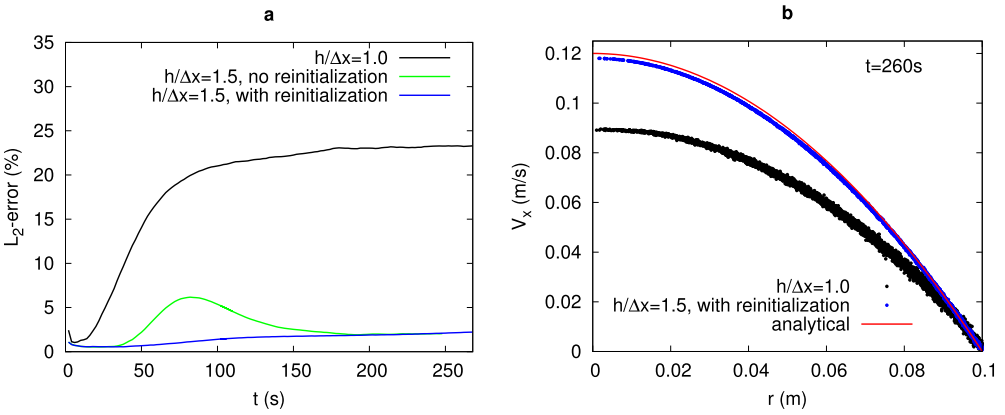

Fig. 9. (Color online) SPH simulation of pipe flow driven by a constant body force at Re $= 120$. (a) Evolution of the L_2 error with and without density re-initialization for $h/\Delta x = \{1, 1.5\}$; (b) velocity profile at time $t = 260$ s obtained from SPH simulation in comparison with the analytical result [22]. The symbols show the streamwise velocity of all SPH particles versus their position in the direction normal to the wall.

In this paper we did not consider artificial viscosity, which on the one hand brings in more free parameters and on the other hand cannot produce correct viscosity at this relatively low Reynolds number regime [23]. We also did not consider particle inconsistency corrections since they are not expected to help in Poiseuille flow simulation [25].

5. Pipe flow

In order to demonstrate that the above arguments are relevant for other wall-shear flows too, herein we study the influence of the smoothing length to particle spacing ratio, $h/\Delta x$, and the density re-initialization scheme for pipe flow at Re $= 120$ which is much larger than usual test cases reported in the literature. The Reynolds number is defined as Re $= UD/\nu$ where U and D are the mean flow speed and pipe diameter, respectively. We assume the following parameters: $D = 0.2$ m, $\rho_0 = 1000\,\mathrm{kg/m^3}$, $\nu = 10^{-4}\,\mathrm{m^2/s}$, pipe length $L = 0.06$ m and the constant driving body force density $f = 4.8 \times 10^{-3}\,\mathrm{m\,s^{-2}}$. The corresponding stationary Hagen–Poiseuille flow with parabolic velocity profile has a peak velocity of 0.12 m/s at the center of the pipe. To model the pipe geometry, we distribute particles on a lattice in a rectangular box and mark particles inside the circular pipe as fluid particles and the rest as wall particles. We only keep wall particles that are within a distance about 3 times the average particle spacing from the pipe wall and use them to impose the no-slip boundary condition at the wall. We choose $h = 0.004$ m, i.e. $h/R = 0.04$ and investigate the effect of density re-initialization and spacing ratio for $h/\Delta x = 1.0$ and $h/\Delta x = 1.5$.

Fig. 9a shows the L_2 error with respect to the analytical solution [22] over time, for different values of $h/\Delta x$, with and without density re-initialization. Similar to Poiseuille flow, we obtain great improvement of the quality of the numerical solutions, expressed by considerable reduction in L_2 when increasing $h/\Delta x$ from 1 to 1.5. Considering the results for $h/\Delta x = 1.5$ (green line in Fig. 9a) we observe a non-monotonous evolution of L_2 which grows up to 7%. This implies the accuracy of the transient solution is clearly worse than the accuracy of the stationary solution which agrees up to $L_2 = 2\%$ with the analytical result. The inability to accurately capture the transient flow is a severe drawback of standard SPH. This problem can be suppressed using the density re-initialization technique

Similar improvement of the result can be observed in Fig. 9b for the velocity profile at time $t = 260$ s (corresponding to 80 convective time units D/U). Increasing $h/\Delta x$ and using density re-initialization does not only yield a velocity profile much closer to the analytical solution but also reduces the noise level significantly.

The deviation of the stationary velocity profile obtained from SPH from the analytical solution, expressed by a finite L_2 value for large time (see Fig. 9a) is partially due to the imperfect modeling of the cylindrical boundary described before. In fact, due to the modeling limitation, the computational domain used for SPH is represented by a pipe with small streamwise groove-like structures with characteristic height and azimuthal separation of about Δx. This roughness perturbs the flow and contributes to the noisy flow field in particular close to the wall boundary; see the broad distribution of the streamwise velocity of particles close to the boundary $r = 0.1$ m in Fig. 9b. Again, we point out that these velocity fluctuations are certainly not due to turbulence since the system operates in a regime far below the lowest Reynolds number at which turbulence can be observed in pipe flow (Re ≈ 1760 [36]).

The results presented in this section show that without a careful parameter choice and the density re-initialization, SPH fails for the simulation of shear flow at low Reynolds number, Re $= 120$.

6. Conclusion

We numerically investigated the stability of SPH simulations with respect to smoothing length h, smoothing length to particle spacing ratio $h/\Delta x$, initial setup of the fluid particles, and density re-initialization. The accuracy of the simulation results was quantified by the L_2-error of the numerical solution with respect to the analytical solution.

Please cite this article in press as: B. Song, et al., Instability of smoothed particle hydrodynamics applied to Poiseuille flows, Computers and Mathematics with Applications (2018), https://doi.org/10.1016/j.camwa.2018.06.037.

In agreement with the literature [22,23,25,26] we found that SPH delivers quantitatively precise results only for the case of very small Reynolds number, e.g., Re $= 0.06$ while it fails dramatically for larger Reynolds number. Proper background pressure could regularize the particle distribution and significantly improve the stability of SPH. However, there is no a priori rule for the choice. our simulations showed that the results sensitively depend on the choice of its value, and we did not observe a systematic convergence as we varied the background pressure. Reducing the smoothing length, h, does not improve the stability of the simulation. However, increasing $h/\Delta x$ for fixed value of h strongly improves the results. For our setup we found that $h/\Delta x \gtrsim 1.5$ is necessary to obtain reliable results for Poiseuille flows at moderate Reynolds numbers (Re $\gtrsim$1). For our system, in contradiction to [23], we did not find any evidence to indicate that lattice configuration of initial particles contributes to the instability; furthermore the irregular initial particle configuration leads to larger error than regular initial positions, in particular during the transient time, while the asymptotic velocity profile was not affected by the initial particle positions. We also showed that density re-initialization is necessary for SPH that adopts continuity equation for density update. This technique reduces density, pressure, and velocity fluctuations in the flow domain, especially in regions far from the wall boundary. To sum up, we argue that the so-called transverse instability [22,23,25] results from the significant dependence of the accuracy of SPH on the regularity of the particle distribution, which in general cannot be assured in simulations. Based on our tests, we found that this instability can be largely avoided by using $h/\Delta x \gtrsim 1.5$ and density re-initialization. In the current paper, we systematically studied flows in a wide range of Reynolds numbers up to Re=120. For larger Reynolds numbers, the computer time increases rapidly due to increasingly restrictive time-step sizes. Some non-systematic preliminary simulations suggest that the technique we used to suppress instabilities works also at larger Reynolds numbers. However, at larger Reynolds numbers it will be difficult to clearly separate the error due to instability of SPH from fluctuations due to the nonlinear instability of the flow itself (turbulence can occur at Reynolds number around 700 [29]). These preliminary results require certainly more detailed investigations which are subject of our future work.

When modeling the domain boundary by means of dummy SPH particles, the boundary velocity and the boundary pressure approximation introduces additional velocity disturbances near the wall. The disturbances gradually propagate to the entire domain, resulting in noisy fields of flow velocity and other hydrodynamic fields. Evidently, modeling the boundaries with discrete particles does not allow for the description of perfectly smooth and impermeable walls. The resulting irregularity due to this approach may be understood as a roughness which in turn may be quantified through the specific boundary condition implementation and the corresponding parameters. We believe that a quantitative description of the *numerical* roughness would allow to apply SPH to the simulations of fluid flow in the vicinity of *physically* rough walls, which is subject of current research.

Acknowledgments

We thank the German Research Foundation (DFG) for funding through the Cluster of Excellence EXC315 "Engineering of Advanced Materials" and German Aerospace Center (DLR) for funding through grant GRANADA. Support from ZISC and IZ-FPS at FAU Erlangen-Nürnberg is gratefully acknowledged. The authors thank Dan Negrut for his comments on a draft of this manuscript.

References

[1] L.B. Lucy, A numerical approach to the testing of the fission hypothesis, Astron. J. 82 (1977) 1013–1024.
[2] R.A. Gingold, J.J. Monaghan, Smoothed particle hydrodynamics: theory and application to non-spherical stars, Mon. Not. R. Astron. Soc. 181 (1977) 375–389.
[3] J.P. Morris, Simulating surface tension with smoothed particle hydrodynamics, Internat. J. Numer. Methods Fluids 33 (2000) 333–353.
[4] A. Colagrossi, M. Landrini, Numerical simulation of interfacial flows by smoothed particle hydrodynamics, J. Comput. Phys. 191 (2003) 448–475.
[5] Z. Wei, et al., SPH modeling of dynamic impact of tsunami bore on bridge piers, Coast. Eng. 104 (2015) 26–42.
[6] Z. Wei, R.A. Dalrymple, E. Rustico, A. Hèrault, G. Bilotta, Simulation of nearshore tsunami breaking by smoothed particle hydrodynamics method, J. Waterw. Port Coastal Ocean Eng. (2016) 05016001.
[7] X.Y. Hu, N.A. Adams, An incompressible multi-phase SPH method, J. Comput. Phys. 227 (2006) 264–278.
[8] S. Adami, X.Y. Hu, N.A. Adams, A transport-velocity formulation for smoothed particle hydrodynamics, J. Comput. Phys. 241 (2013) 292–307.
[9] S. Adami, X.Y. Hu, N.A. Adams, A generalized wall boundary condition for smoothed particle hydrodynamics, J. Comput. Phys. 231 (2012) 7057–7075.
[10] A. Pazouki, D. Negrut, A numerical study of the effect of particle properties on the radial distribution of suspensions in pipe flow, Comput. & Fluids 108 (2014) 1–12.
[11] A. Pazouki, D. Negrut, Numerical investigation of microfluidic sorting of microtissues, Comput. Math. Appl. 72 (2016) 251–263.
[12] A. Mayrhofer, D. Laurence, B.D. Rogers, D. Violeau, DNS and LES of 3-d wall-bounded turbulence using smoothed particle hydrodynamics, Comput. & Fluids 115 (2015) 86–97.
[13] J.J. Monaghan, Smoothed particle hydrodynamics, Rep. Progr. Phys. 68 (2005) 1703–1759.
[14] M.B. Liu, G.R. Liu, Smoothed particle hydrodynamics (SPH): an overview and recent developments, Arch. Comput. Methods Eng. 17 (2010) 25–76.
[15] J.J. Monaghan, Smoothed particle hydrodynamics and its diverse application, Annu. Rev. Fluid Mech. 44 (2012) 323–346.
[16] S.J. Cummins, M. Rudman, An SPH projection method, J. Comput. Phys. 152 (1999) 584–607.
[17] X.Y. Hu, N.A. Adams, An incompressible multi-phase SPH method, J. Comput. Phys. 227 (2007) 264–278.
[18] R. Xu, P. Stansby, D. Laurence, Accuracy and stability in incompressible SPH (iSPH) based on the projection method and a new approach, J. Comput. Phys. 228 (2009) 6703–6725.
[19] K. Bodin, C. Lacoursiére, M. Servin, Constraint fluids, IEEE Trans. Vis. Comput. Graphics 18 (3) (2012) 516–526.
[20] M. Ihmsen, J. Cornelis, B. Solenthaler, C. Horvath, M. Teschner, Implicit incompressible SPH, IEEE Trans. Vis. Comput. Graphics 20 (3) (2014) 426–435.
[21] J.P. Morris, P.J. Fox, Y. Zhu, Modeling low Reynolds number incompressible flows using SPH, J. Comput. Phys. 136 (1997) 214–226.

Please cite this article in press as: B. Song, et al., Instability of smoothed particle hydrodynamics applied to Poiseuille flows, Computers and Mathematics with Applications (2018), https://doi.org/10.1016/j.camwa.2018.06.037.

[22] L.D.G. Sigalotti, J. Klapp, E. Sira, Y. Meleán, A. Hasmy, SPH simulations of time-dependent Poiseuille flow at low Reynolds numbers, J. Comput. Phys. 191 (2003) 622–638.
[23] M. Meister, G. Burger, W. Rauch, On the Reynolds number sensitivity of smoothed particle hydrodynamics, J. Hydraul. Res. 52 (2014) 824–835.
[24] Y. Imaeda, S.-I. Inutsuka, Shear flows in smoothed particle hydrodynamics, Astrophys. J. 569 (2002) 501–518.
[25] M. Basa, N.J. Quinlan, M. Lastiwka, Robustness and accuracy of SPH formulations for viscous flow, Internat. J. Numer. Methods Fluids 60 (2009) 1127–1148.
[26] S.J. Watkins, A.S. Bhattal, N. Francis, J.A. Turner, A.P. Whitworth, A new prescription for viscosity in smoothed particle hydrodynamics, Astron. Astrophys. Suppl. Ser. 119 (1996) 177–187.
[27] P. Tamamidis, G. Zhang, D.N. Assanis, Comparison of pressure-based and artificial compressibility methods for solving three-dimensional steady incompressible viscous flows, J. Comput. Phys. 124 (1996) 1.
[28] N. Tofighi, M. Ozbulut, A. Rahmat, J.J. Feng, M. Yildiz, An incompressible smoothed particle hydrodynamics method for the motion of rigid bodies in fluids, J. Comput. Phys. 297 (2015) 207–220.
[29] L.S. Tuckerman, T. Kreilos, H. Schrobsdorff, T.M. Schneider, J.F. Gibson, Turbulent-laminar patterns in plane poiseuille flow, Phys. Fluids 26 (2014) 114103.
[30] M.B. Liu, G.R. Liu, Restoring particle consistency in smoothed particle hydrodynamics, Appl. Numer. Math. 56 (2006) 19–36.
[31] J.J. Monaghan, SPH without a tensile instability, J. Comput. Phys. 159 (2000) 290–311.
[32] M. Ellero, N.A. Adams, SPH simulations of flow around a periodic array of cylinders confined in a channel, Internat. J. Numer. Methods Engrg. 86 (2011) 1027–1040.
[33] A. Colagrossi, B. Bouscasse, M. Antuono, S. Marrone, Particle packing algorithm for SPH schemes, Comput. Phys. Comm. 183 (2012) 1641–1653.
[34] M. Kondo, S. Koshizuka, Improvement of stability in moving particle semi-implicit method, Internat. J. Numer. Methods Fluids 65 (2011) 638–654.
[35] Y. Huang, C. Zhu, Simulation of flow slides in municipal solid waste dumps using a modified MPS method, Nat. Hazards 74 (2014) 491–508.
[36] R.R. Kerswell, Recent progress in understanding the transition to turbulence in a pipe, Nonlinearity 18 (2005) R17–R44.

Please cite this article in press as: B. Song, et al., Instability of smoothed particle hydrodynamics applied to Poiseuille flows, Computers and Mathematics with Applications (2018), https://doi.org/10.1016/j.camwa.2018.06.037.